# *Tuning the Excitonic Properties of the 2D (PEA) 2 (MA) n −1 Pb n I 3 n +1 Perovskite Family via Quantum Confinement*



**As Published:** 10.1021/acs.jpclett.0c03731

**Publisher:** American Chemical Society (ACS)

**Persistent URL:** https://hdl.handle.net/1721.1/134117

**Version:** Author's final manuscript: final author's manuscript post peer review, without publisher's formatting or copy editing

# Quantum confinement as a tool to tune the excitonic properties of the $(PEA)_2(MA)_{n-1}Pb_nI_{3n+1}$ family of 2D perovskites

Mateusz Dyksik,[†,‡] Shuli Wang,[†] Watcharaphol Paritmongkol,[¶,§] Duncan K. Maude,[†] William A. Tisdale,[*,¶] Michal Baranowski,[*,‡] and Paulina Plochocka[*,†,‡]

†*Laboratoire National des Champs Magnétiques Intenses, UPR 3228, CNRS-UGA-UPS-INSA, Grenoble and Toulouse, France*

‡*Department of Experimental Physics, Faculty of Fundamental Problems of Technology, Wroclaw University of Science and Technology, Wroclaw, Poland*

¶*Department of Chemical Engineering, Massachusetts Institute of Technology, Cambridge, Massachusetts 02139, United States*

§*Department of Chemistry, Massachusetts Institute of Technology, Cambridge, Massachusetts 02139, United States*

E-mail: tisdale@mit.edu; michal.baranowski@pwr.edu.pl; paulina.plochocka@lncmi.cnrs.fr

**Abstract**

In atomically thin 2D crystals, the excitonic properties and band structure scale strongly with the thickness, providing a new playground for the investigation of exciton physics in the ultimate confinement regime. Here, we demonstrate the evolution of the fundamental excitonic properties, such as reduced mass, wave function extension and exciton binding energy, in the 2D perovskite $(PEA)_2(MA)_{n-1}Pb_nI_{3n+1}$, for $n = 1, 2, 3$. These parameters are experimentally determined using optical spectroscopy in high magnetic field up to 65 T. The observation of the inter band Landau level transitions provides direct access to the reduced effective mass $\mu$ and band gap $E_g$. We show that $\mu$ increases with the number of inorganic sheets $n$, reaching the value of 3D $MAPbI_3$ already for $n = 3$. Our experimental observations contradict the general expectation that quantum confinement leads to an enhanced carrier mass, showing another aspect of the unprecedented flexibility in the design of the electronic properties of 2D perovskites.

# Graphical TOC Entry

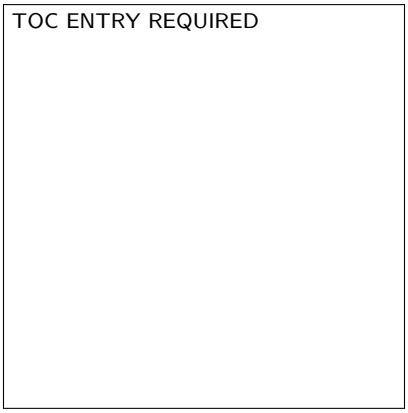

Two-dimensional metal-halide perovskites constitute an important step in the evolution of low-cost organic-inorganic hybrid light absorbers and emitters.[1–5] Similar to their 3D counterparts, layered perovskites show promising performance in photovoltaic and light emitting devices,[6–9] while preserving high environmental stability.[7,10] The latter is of paramount importance for the industrialization of perovskite technology.

In 2D perovskites the improved stability stems from the large hydrophobic organic cations $L$ separating inorganic octahedra sheets. The general formula describing Ruddlesden-Popper (RP) 2D layered perovskites is $L_2A_{n-1}M_nX_{3n+1}$, where A is a small monovalent cation, M is a metal atom, X is a halide atom and $n$ denotes the number of octahedral layers. In contrast to their 3D counterparts ($AMX_3$), where A cannot be chosen arbitrarily, in 2D perovskites there is a wide choice of the organic spacer L, including aliphatic chains, benzene-like molecules with different substitutions and many others.[1,11–13] This makes 2D perovskites an unprecedented material system regarding the tuning flexibility of the opto-electronic properties. Large organic spacers $L$ provide control over the dielectric confinement[14–17] as well as the crystal and band structure[1,2,5,18,19] and, as a result, the carrier effective mass.[20,21] The carrier mass can be substantially modified by the octahedral layer thickness,[20] structural phase transitions[21] or cation composition.[22]

2D lead-based perovskites with phenethylamine (PEA, $C_6H_5C_2H_4NH_3$) as a organic spacers, namely $(PEA)_2MA_{n-1}Pb_nI_{3n+1}$ (where MA stands for methylammonium) are one of the most studied systems. They are often considered as a reference structure to understand the influence of L on the opto-electronic properties of 2D perovskites.[12,13,23] Despite their popularity and successfully deployment in various opto-electronic devices,[10,24,25] some questions about their fundamental opto-electronic properties remain unanswered. For example, determining the effective mass of charge carriers in 2D perovskites is challenging, with most attempts so far limited to density functional theory (DFT) calculations[26–28] which are known to have limited accuracy without experimental support.[29] It is also interesting to understand how the carrier effective mass changes with increasing $n$, as the crystal structure evolves from

that imposed by the large organic spacer L, to the crystal structure determined mostly by MA *i.e* in the bulk limit. Currently, the only report addressing this problem is limited to the case of butylamine (BA).[20] It was shown that the carrier effective mass is enhanced in this 2D perovskite with respect to 3D $MAPbI_3$, and with an increasing number of inorganic sheets $n$, the effective mass $\mu$ decreases, reaching the bulk limit for high $n$ values.

Here we demonstrate that such an observation does not necessarily apply to all 2D perovskites. Using optical spectroscopy in high magnetic fields, we observe inter band Landau level transitions which provide direct access to the reduced effective mass $\mu$ of charge carriers in $(PEA)_2MA_{n-1}Pb_nI_{3n+1}$ 2D perovskites, where $n = 1, 2, 3$. We demonstrate that $\mu$ increases with the number of inorganic layers $n$, reaching the same value as 3D $MAPbI_3$ already for $n = 3$. Our observations, and previous experimental reports[20,22] prove that an appropriate choice of organic spacer and inorganic layer thickness provide efficient methods to engineer the carrier effective mass in 2D perovskites, which can be either lower or higher than in their 3D analogues. Having precisely determined $\mu$ we then report on all important exciton parameters, such as binding energy and in-plane radius, and how these parameters evolve with increasing $n$. Our experimentally determined parameters can serve as a benchmark for first principles calculations and exciton models.

The optical spectroscopy measurements were performed on a series of three perovskite crystals $(PEA)_2MA_{n-1}Pb_nI_{3n+1}$, where $n = 1, 2, 3$ (*i.e.* $(PEA)_2PbI_4$, $(PEA)_2MAPb_2I_7$ and $(PEA)_2MA_2Pb_3I_{10}$ (see Methods section for more details on sample preparation and experimental techniques). Figure 1 summarizes the optical response (reflectivity (R) and photoluminescence (PL)) for each sample in the spectral range of the 1s excitonic transition, measured at 4.2 K. The reflectivity spectra (solid lines in panels a-c) show multiple absorption minima characteristic of phonon replicas.[30,31] The photoluminescence response (shaded curves) from the respective crystals are a "mirror image" of the absorption (Fig. S1).[30]

In the presence of external magnetic field, the 1s exciton transition blue shifts for all three crystals, which can be seen in the false-color maps in Fig. 1 (d-f). When the cyclotron

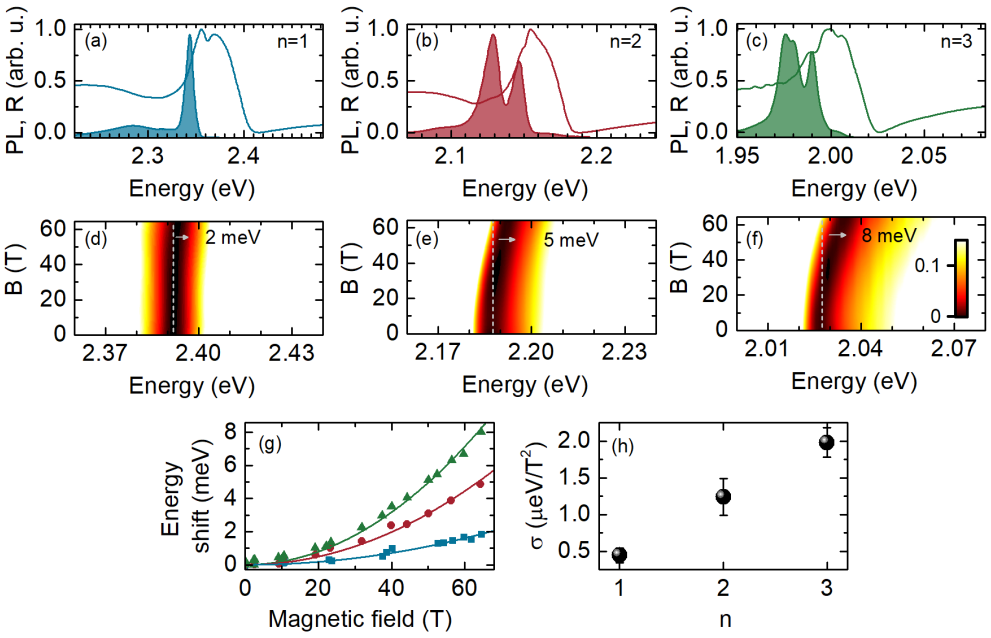


Figure 1: (a-c) Steady-state optical response, reflectivity (solid) and photoluminescence (shaded), in the spectral range of the 1s exciton for $n = 1, 2, 3$ crystals. Panels (d-e) show the evolution of the 1s exciton in the presence of external magnetic field. Data points in panel (g) represent the 1s transition energy extracted for several magnetic field values whereas solid lines are fits using Eq. 1. (h) The diamagnetic coefficients $\sigma$ versus the number of inorganic sheets $n$.

energy of carriers in a magnetic field is much lower than the exciton binding energy, the transition energy shifts quadratically in the magnetic field according to,

$$\Delta E = \sigma B^2, \tag{1}$$

where the diamagnetic coefficient $\sigma$ depends only on the exciton reduced mass $\mu$ and root mean square (rms) wave function extension $\sqrt{\langle r^2 \rangle}$,

$$\sigma = \frac{e^2}{8\mu} \langle r^2 \rangle. \tag{2}$$

The extracted energy shift in magnetic field (Fig. 1g) is well described by Eq. 1, providing a precise determination of the diamagnetic coefficient $\sigma$ for each crystal. The evolution of $\sigma$ with number of inorganic sheets $n$ is summarized in Fig. 1(h) and is in agreement with our previous work on thin films.[31]

In the high energy range of the reflectivity spectra, we observe the formation of Landau levels in each sample. To better visualize this in Fig 2(a-c), reflectivity ratio spectra are presented (*i.e.*, spectra measured at a high magnetic field divided by the zero-field spectrum). In each case we observe several equally-spaced spectral features (labeled LL0, LL1...) which we ascribe to optical transition between Landau levels induced by the magnetic field. Each minimum in the R(B)/R(0) spectrum strengthens, and shifts towards higher energies as the magnetic field increases, corroborating our interpretation. Remarkably, this finding shows that electron and hole states in 2D perovskites are quantized into Landau levels in the presence of sufficiently strong magnetic field. Each Landau level is described by its orbital quantum number $N$, as schematically depicted in Fig. 2(g). Optical transition are dipole allowed between conduction and valance band states with the same $N$. The energy corresponding to the minimum of each feature in the ratio spectra is thus the inter band transition energy between the valence and conduction band Landau levels with the same $N$.[32]

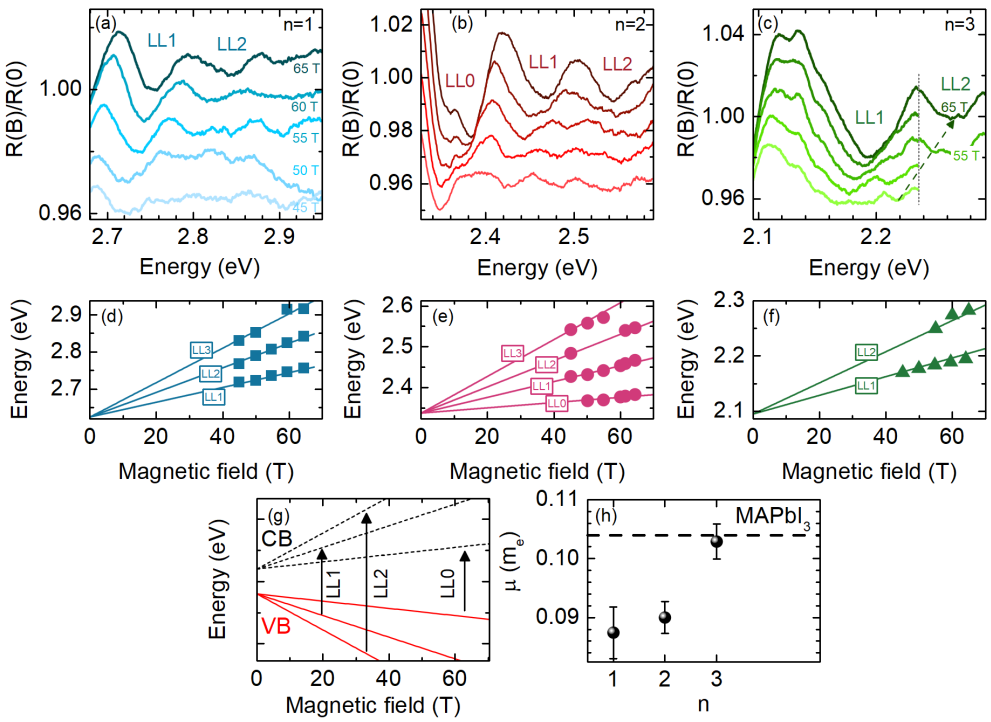


Figure 2: (a-c) R(B)/R(0) reflectivity ratio spectra for $n = 1, 2, 3$ crystals, respectively. The magnetic field strengths indicated in panel (a), apply for all three panels. Labels LLN, $N = 0, 1, 2..$ enumerate the interband Landau level transitions. The evolution of each optical transition as a function of magnetic field is plotted in panels (d-f) in the form of fan charts. (g) Only optical transitions between the valence band (VB) and conduction band (CB) states with the same orbital quantum number $N$ are dipole allowed. Solid lines in panels (d-f) are fits to the Landau level transitions using Eq. 3 which provides the values of reduced effective mass $\mu$ plotted as a function of $n$ in (h). In panel (c) the dotted line separates two different data sets and the dashed arrow is a guide to the eye.

Assuming a parabolic band dispersion, the energy of inter band Landau levels transitions are given by,

$$E_N(B) = E_g + \Big(N + \frac{1}{2}\Big)\hbar\omega_c, \tag{3}$$

where $E_g$ is the band gap, $N = 0, 1, 2, \ldots$ represents the Landau orbital quantum number in the conduction and valence band, $\hbar\omega_c = eB/\mu$ is the combined (electron + hole) cyclotron energy and $\mu^{-1} = m_e^{-1} + m_h^{-1}$ is the exciton reduced mass ($m_e$ and $m_h$ are the effective masses for electrons and holes, respectively). Fig. 2(d-f) summarizes the evolution of the $N$-th Landau level transition energies for the $n = 1, 2, 3$ crystals.

Using Eq. 3 we fit the experimental points in panels (d-f) to extract the reduced effective mass $\mu$ and the band gap energy $E_g$. The obtained values of $\mu$ increase with the number of inorganic layers $n$ (0.087 $\pm$ 0.004, 0.090 $\pm$ 0.003 and 0.103 $\pm$ 0.003, for the $n = 1, 2, 3$ crystals (in units of the free electron mass), see Tab. 1). As $n$ increases, the initially 2D layered crystals transform into a more 3D-like (bulk) structures. Hence, it is natural that the charge carrier properties follow the structural transformation and also tend to approach 3D values with increasing $n$.

Although the effective mass $\mu$ indeed approaches the value for bulk $MAPbI_3$ (Fig. 2h), the increase in $\mu$ with increasing $n$ is in striking contrast to what is known for fully inorganic epitaxial quantum wells[33–37] and BA-based 2D perovskites,[20] where the reduction of quantum well width leads to an enhancement of $\mu$. The experimentally observed trend is also in contrast to the theoretically estimated behaviour for PEA-containing 2D perovskites,[38] where $\mu$ is reduced while $n$ increases, very similar to the BA case.[39] Clearly, the resulting confusion in the literature regarding the estimated values of effective mass requires clarification by direct experimental measurements, which in turn could contribute to improvements of available theoretical models.

Our results clearly show that 2D perovskites constitute a novel material system where the carrier effective mass in low dimensional structures can be either lower or higher than for the 3D counterparts, even though the bands are built primarily from the same atoms of

$PbI_6$ octahedral units. All these findings point to the importance of the templating effect[18] (imposed by organic spacers), which not only affect the band gap but is also reflected in the band dispersion and all related quantities. In the case of 2D perovskites with $n = 1$, the simple correlation between carrier effective mass and the in- and out-of-plane distortion of the octahedral units can be drawn,[21,22] where the effective mass $\mu$ is larger for structures with higher distortions. In the case of $n = 2$ and 3 the structure of the octahedral layer and the angles describing its geometry are much more complex *i.e.* the octahedra distortion can be different for consecutive inorganic sheets.[40] Furthermore, the lack of low temperature crystallographic data for $n = 2, 3$ crystals prevents us from finding a direct correlation between the octahedra distortion and the observed reduced effective mass. However, it is well-known that PEA organic spacer imposes a low degree of corrugation on the inorganic framework,[23,41,42] much lower than for example the aliphatic chains (*i.e.* n-butylamine[40,43]). The out-of-plane distortion $\delta$ (Fig. S2) for $n = 1$ ($\delta < 2$) is even lower than for 3D $MAPbI_3$ ($\delta > 3$, distortion mapped from orthorhombic phase assuming the stacking direction is along the $c$ axis[44]). Taking into account that all excitonic parameters studied within this work are approaching the 3D $MAPbI_3$ values with increasing $n$, this observation provides a guideline as to how distortions would be affected by increasing $n$.

**Table 1: Material parameters determined in this work; (from left) band gap energy, exciton binding energy, rms radius, and reduced effective mass. The data for the $MAPbI_3$ crystal are taken from previous magneto-absorption measurements reported by Miyata *et al.*[45]**

| | $E_g$ (eV) | $E_b$ (meV) | $\sqrt{\langle r^2 \rangle}$ (nm) | $\mu$ ($m_e$) |
|---|---|---|---|---|
| $(PEA)_2PbI_4$ | 2.625 | 265 | 1.3 | 0.087 |
| $(PEA)_2(MA)Pb_2I_7$ | 2.337 | 162 | 2.3 | 0.090 |
| $(PEA)_2(MA)_2Pb_3I_{10}$ | 2.09 | 78 | 3 | 0.103 |
| $MAPbI_3$ | 1.65 | 16[45] | $\sim 8$ | 0.104[45] |

The observation of Landau levels also allows for a precise determination of the the band gap energy. It is important to note that determining the band gap from the absorption spectrum is quite arbitrary, since the line-shape of the absorption spectrum close to the

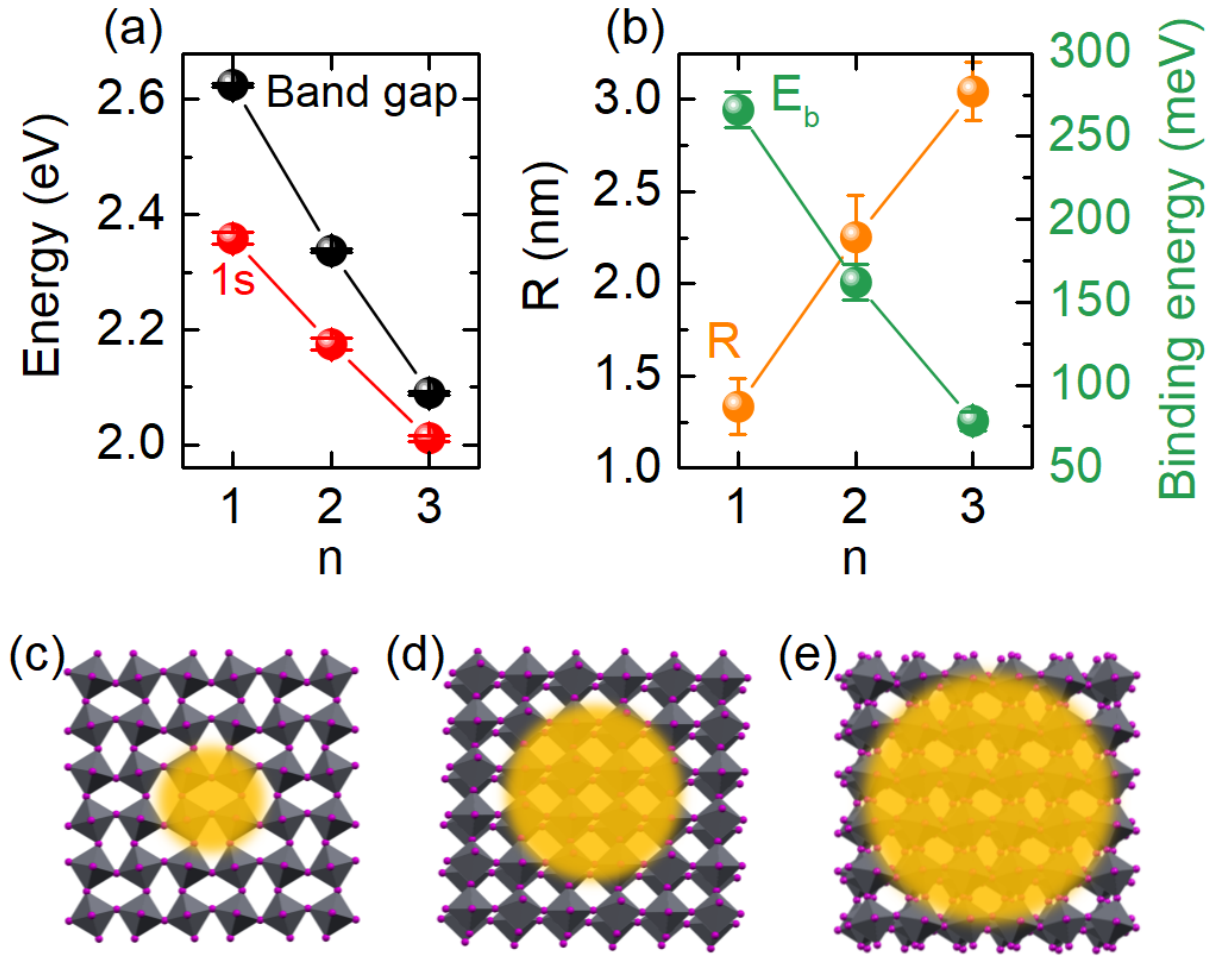


Figure 3: (a) Band gap and 1s exciton energies as a function of an increasing number of inorganic octahedra sheets $n$. The band gap energy is obtained by fitting data points in Fig. 2(d-f) with Eq. 3. (b) The exciton rms radius (left axis) and exciton binding energy ($E_b$=$E_g$-$E_{1s}$) as a function of $n$. Panels (c-e) schematically depict the exciton wave-function extension in the plane of the inorganic sheets for $n = 1, 2, 3$ crystals

band edge can be affected by high energy excitonic states or the Urbach tail. In contrast, the Landau level energies intersect at $E_g$ (Fig. 2d-f) when the magnetic field $B \to 0$, providing a better estimation of $E_g$ as more Landau level transitions are observed. Figure 3(a) shows the evolution of the extracted band gaps together with the 1s exciton energies for all three crystals. Similar to $\mu$, $E_g$ moves closer to the band gap value of $MAPbI_3$ ($\sim$1.65 eV) when the number of inorganic sheets $n$ increases from 1 to 3 in the $(PEA)_2(MA)_{n-1}Pb_nI_{3n+1}$. The obtained values of band gap and 1s exciton energies determine the exciton binding energies $E_b$ of 265, 162 and 78 meV for $n = 1, 2, 3$ crystals, respectively. All values of $E_g$, $E_b$, $\mu$ are summarized in Tab. 1. For $n = 1$ we can see that the extracted $E_b$ is in the upper range of reported values.[14,30,31,46,47] This might indicate that the value of $E_g$ was often underestimated from the onset of the absorption spectrum.

The extracted excitons binding energies indicate the importance of dielectric screening for all $n$, and the non-hydrogenic nature of excitons in 2D perovskites. Indeed, the transformation of the pure-hydrogen model from 3D to 2D should result in a fourfold increase of the exciton binding energy. Even though the extracted $\mu$ are lower or the same as for $MAPbI_3$ for all $n$, the binding energy $E_B$ is higher than 64 meV ($4 \times E_b$ of $MAPbI_3$), pointing to the importance of the dielectric confinement effect.

Having determined $\mu$, we can now use eq. 2 to estimate the 1s exciton root-mean-square (rms) radius in the plane of the octachedral sheets. We find the 1s rms radius of $1.33 \pm 0.15$ nm for the $n = 1$ sample, which increases to $2.25 \pm 0.23$ nm and $3.04 \pm 0.16$ nm for samples with $n = 2$ and $n = 3$, respectively (Fig. 3b). Fig. 3(c-e) schematically depicts the 1s exciton wavefunction extension as the number of inorganic sheets increases from 1 to 3. For comparison, 3D $MAPbI_3$, with a binding energy of 16 meV in the orthorhombic phase,[48] shows an exciton rms radius of $\simeq$ 8 nm ($\sqrt{3}\,a_B$, where $a_B$ is the Bohr radius). All of the extracted parameters show a gradual progression towards the 3D values with increasing $n$. However only $\mu$ reaches bulk value for $n = 3$. This is because band dispersion and effective mass are predominantly related to the lattice structure and overlap of atomic

orbitals,[22] while the remaining quantities are in addition strongly affected by the quantum and dielectric confinement.

To summarize, we have determined the basic excitonic parameters for the PEA-based metal-halide 2D perovskites with a different number of inorganic sheets $n$. We have investigated three crystals ($n = 1, 2, 3$) from the $(PEA)_2(MA)_{n-1}Pb_nI_{3n+1}$ material family. Using optical spectroscopy in high magnetic fields, we observe inter band Landau level transitions in the above band gap spectral range, providing a direct and precise value of the reduced effective mass $\mu$ of the exciton. The determined reduced effective mass for the $n = 1$ crystal equals to $0.087 \pm 0.004$ $m_e$ and increases with number of inorganic layers to reach the value of 3D $MAPbI_3$ already for $n = 3$. Moreover, an analysis of the Landau level transitions allows a precise determination of the band gap, giving direct access to the exciton binding energy. Furthermore, having precisely determined the $\mu$ and the diamagnetic shift of the 1s exciton, we can estimate the in-plane root-mean-square values of the exciton wave function, and how it evolves with the number of inorganic sheets $n$. Importantly, all of these parameters were extracted experimentally, and can serve as benchmark for band structure and exciton models in this challenging material system.

# Experimental Methods

To access the properties of the 1s excitons, such as the reduced effective mass $\mu$ and rms size $\langle r^2 \rangle$ we have performed a comprehensive magneto-reflectivity measurements. Three perovskite crystals $(PEA)_2MA_{n-1}Pb_nI_{3n+1}$ with $n = 1, 2, 3$ (ie $(PEA)_2PbI_4$, $(PEA)_2MAPb_2I_7$ and $(PEA)_2MA_2Pb_3I_{10}$, abbreviated as $n = 1, 2, 3$ throughout this work, have been prepared as pure phases by the cooling induced crystallization method[40,49] (see Supporting Information).

The reflectance (R) measurements were performed in a back scattering geometry in a liquid helium cryostat placed in the bore of a pulsed magnet.[50] A broad band white light

source was provided by a tungsten halogen lamp and transmitted to the sample using an optical fiber. The reflected light was collected by a fiber bundle, which surrounds the excitation fiber. The same setup was used for photoluminescence (PL) measurements. The reflected light, or the PL signal, were analyzed by an optical spectrometer (30 or 50 cm long) equipped with a liquid nitrogen cooled CCD camera. Magnetic field measurements up to 65 T were performed in the Faraday configuration in a pulsed magnet, with a pulse duration of $\simeq 300$ ms. All measurements, unless otherwise stated, were performed with the sample at $T = 2.2$ K.

## Acknowledgements

This project has received funding from National Science Centre Poland within the OPUS program (grant no. 2019/33/B/ST3/01915). This work was partially supported by OPEP project, which received funding from the ANR-10-LABX-0037-NEXT. M.D. appreciates support from the Polish National Agency for Academic Exchange within the Bekker programme (grant no. PPN/BEK/2019/1/00312/U/00001). The Polish participation in European Magnetic Field Laboratory is supported by the DIR/WK/2018/07 grant from Ministry of Science and Higher Education, Poland. Materials synthesis and characterization at MIT was supported by the U.S. Department of Energy, Office of Science, Basic Energy Sciences, under award no. DE-SC0019345.

## Supporting Information

## References

(1) Chen, Y.; Sun, Y.; Peng, J.; Tang, J.; Zheng, K.; Liang, Z. 2D Ruddlesden–Popper perovskites for optoelectronics. *Adv. Mater.* **2018**, *30*, 1703487.

(2) Pedesseau, L.; Sapori, D.; Traore, B.; Robles, R.; Fang, H.-H.; Loi, M. A.; Tsai, H.; Nie, W.; Blancon, J.-C.; Neukirch, A. et al. Advances and promises of layered halide hybrid perovskite semiconductors. *ACS Nano* **2016**, *10*, 9776–9786.

(3) Yan, J.; Qiu, W.; Wu, G.; Heremans, P.; Chen, H. Recent progress in 2D/quasi-2D layered metal halide perovskites for solar cells. *J. Mater. Chem.A* **2018**, *6*, 11063–11077.

(4) Mao, L.; Ke, W.; Pedesseau, L.; Wu, Y.; Katan, C.; Even, J.; Wasielewski, M. R.; Stoumpos, C. C.; Kanatzidis, M. G. Hybrid Dion–Jacobson 2D lead iodide perovskites. *J. Am. Chem. Soc.* **2018**, *140*, 3775–3783.

(5) Straus, D. B.; Kagan, C. R. Electrons, excitons, and phonons in two-dimensional hybrid perovskites: connecting structural, optical, and electronic properties. *J. Phys. Chem. Lett.* **2018**, *9*, 1434–1447.

(6) Blancon, J.-C.; Tsai, H.; Nie, W.; Stoumpos, C. C.; Pedesseau, L.; Katan, C.; Kepenekian, M.; Soe, C. M. M.; Appavoo, K.; Sfeir, M. Y. et al. Extremely efficient internal exciton dissociation through edge states in layered 2D perovskites. *Science* **2017**, *355*, 1288–1292.

(7) Tsai, H.; Nie, W.; Blancon, J.-C.; Stoumpos, C. C.; Asadpour, R.; Harutyunyan, B.; Neukirch, A. J.; Verduzco, R.; Crochet, J. J.; Tretiak, S. et al. High-efficiency two-dimensional Ruddlesden–Popper perovskite solar cells. *Nature* **2016**, *536*, 312–316.

(8) Fu, W.; Wang, J.; Zuo, L.; Gao, K.; Liu, F.; Ginger, D. S.; Jen, A. K.-Y. Two-dimensional perovskite solar cells with 14.1% power conversion efficiency and 0.68% external radiative efficiency. *ACS Energy Lett.* **2018**, *3*, 2086–2093.

(9) Shao, S.; Duim, H.; Wang, Q.; Xu, B.; Dong, J.; Adjokatse, S.; Blake, G. R.; Protesescu, L.; Portale, G.; Hou, J. et al. Tuning the energetic landscape of Ruddlesden–Popper perovskite Films for efficient solar cells. *ACS Energy Lett.* **2020**, *5*, 39–46.

(10) Smith, I. C.; Hoke, E. T.; Solis-Ibarra, D.; McGehee, M. D.; Karunadasa, H. I. A layered hybrid perovskite solar-cell absorber with enhanced moisture stability. *Angew. Chem. Int. Ed.* **2014**, *53*, 11232–11235.

(11) Sichert, J. A.; Hemmerling, A.; Cardenas-Daw, C.; Urban, A. S.; Feldmann, J. Tuning the optical bandgap in layered hybrid perovskites through variation of alkyl chain length. *APL Mater.* **2019**, *7*, 041116.

(12) Straus, D. B.; Iotov, N.; Gau, M. R.; Zhao, Q.; Carroll, P. J.; Kagan, C. R. Longer cations increase energetic disorder in excitonic 2D hybrid perovskites. *J. Phys. Chem. Lett.* **2019**, *10*, 1198–1205.

(13) Tailoring hot exciton dynamics in 2D hybrid perovskites through cation modification. *ACS Nano* **2020**, *14*, 3621–3629.

(14) Hong, X.; Ishihara, T.; Nurmikko, A. Dielectric confinement effect on excitons in PbI 4-based layered semiconductors. *Phys. Rev. B* **1992**, *45*, 6961.

(15) Even, J.; Pedesseau, L.; Katan, C. Understanding quantum confinement of charge carriers in layered 2D hybrid perovskites. *ChemPhysChem* **2014**, *15*, 3733–3741.

(16) Cheng, B.; Li, T.-Y.; Maity, P.; Wei, P.-C.; Nordlund, D.; Ho, K.-T.; Lien, D.-H.; Lin, C.-H.; Liang, R.-Z.; Miao, X. et al. Extremely reduced dielectric confinement in two-dimensional hybrid perovskites with large polar organics. *Communications Physics* **2018**, *1*.

(17) Passarelli, J. V.; Mauck, C. M.; Winslow, S. W.; Perkinson, C. F.; Bard, J. C.; Sai, H.; Williams, K. W.; Narayanan, A.; Fairfield, D. J.; Hendricks, M. P. et al. Tunable exciton binding energy in 2D hybrid layered perovskites through donor–acceptor interactions within the organic layer. *Nat. Chem.* **2020**, *12*, 672–682.

(18) Knutson, J. L.; Martin, J. D.; Mitzi, D. B. Tuning the band gap in hybrid tin iodide perovskite semiconductors using structural templating. *Inorg. Chem.* **2005**, *44*, 4699–4705.

(19) Smith, M. D.; Karunadasa, H. I. White-light emission from layered halide perovskites. *Acc. Chem. Res.* **2018**, *51*, 619–627.

(20) Blancon, J.-C.; Stier, A. V.; Tsai, H.; Nie, W.; Stoumpos, C. C.; Traore, B.; Pedesseau, L.; Kepenekian, M.; Katsutani, F.; Noe, G. et al. Scaling law for excitons in 2D perovskite quantum wells. *Nat. Commun.* **2018**, *9*, 1–10.

(21) Baranowski, M.; Zelewski, S. J.; Kepenekian, M.; Traoré, B.; Urban, J. M.; Surrente, A.; Galkowski, K.; Maude, D. K.; Kuc, A.; Booker, E. P. et al. Phase transition induced carrier mass enhancement in 2D Ruddlesden–Popper perovskites. *ACS Energy Lett.* **2019**, *4*, 2386–2392.

(22) Dyksik, M.; Duim, H.; Zhu, X.; Yang, Z.; Gen, M.; Kohama, Y.; Adjokatse, S.; Maude, D. K.; Loi, M. A.; Egger, D. A. et al. Broad tunability of carrier effective masses in two-dimensional halide perovskites. *ACS Energy Lett.* **2020**, *5*, 3609–3616.

(23) Du, K.-z.; Tu, Q.; Zhang, X.; Han, Q.; Liu, J.; Zauscher, S.; Mitzi, D. B. Two-dimensional lead (II) halide-based hybrid perovskites templated by acene alkylamines: crystal structures, optical properties, and piezoelectricity. *Inorg. Chem.* **2017**, *56*, 9291–9302.

(24) Yu, J.; Kong, J.; Hao, W.; Guo, X.; He, H.; Leow, W. R.; Liu, Z.; Cai, P.; Qian, G.; Li, S. et al. Broadband extrinsic self-trapped exciton emission in Sn-Doped 2D lead-halide perovskites. *Adv. Mater.* **2018**, *31*, 1806385.

(25) Ban, M.; Zou, Y.; Rivett, J. P. H.; Yang, Y.; Thomas, T. H.; Tan, Y.; Song, T.; Gao, X.; Credgington, D.; Deschler, F. et al. Solution-processed perovskite light emitting diodes

with efficiency exceeding 15% through additive-controlled nanostructure tailoring. *Nat. Commun.* **2018**, *9*, 3892.

(26) Even, J.; Pedesseau, L.; Dupertuis, M.-A.; Jancu, J.-M.; Katan, C. Electronic model for self-assembled hybrid organic/perovskite semiconductors: Reverse band edge electronic states ordering and spin-orbit coupling. *Phys. Rev. B* **2012**, *86*, 205301.

(27) Qian, J.; Guo, Q.; Liu, L.; Xu, B.; Tian, W. A theoretical study of hybrid lead iodide perovskite homologous semiconductors with 0D, 1D, 2D and 3D structures. *J. Mater. Chem.A* **2017**, *5*, 16786–16795.

(28) Silver, S.; Yin, J.; Li, H.; Brédas, J.-L.; Kahn, A. Characterization of the valence and conduction band levels of n= 1 2D perovskites: a combined experimental and theoretical investigation. *Adv. Energy Mater.* **2018**, *8*, 1703468.

(29) Crowley, J. M.; Tahir-Kheli, J.; Goddard III, W. A. Resolution of the band gap prediction problem for materials design. *J. Phys. Chem. Lett.* **2016**, *7*, 1198–1203.

(30) Straus, D. B.; Hurtado Parra, S.; Iotov, N.; Gebhardt, J.; Rappe, A. M.; Subotnik, J. E.; Kikkawa, J. M.; Kagan, C. R. Direct observation of electron–phonon coupling and slow vibrational relaxation in organic–inorganic hybrid perovskites. *J. Am. Chem. Soc.* **2016**, *138*, 13798–13801.

(31) Urban, J. M.; Chehade, G.; Dyksik, M.; Menahem, M.; Surrente, A.; Trippé-Allard, G.; Maude, D. K.; Garrot, D.; Yaffe, O.; Deleporte, E. et al. Revealing excitonic phonon coupling in $(PEA)_2(MA)_{n-1}Pb_nI_{3n+1}$ 2D layered perovskites. *J. Phys. Chem. Lett.* **2020**, *11*, 5830–5835.

(32) Miura, N. *Physics of semiconductors in high magnetic fields*; Oxford University Press, 2008; Vol. 15.

(33) Nag, B.; Mukhopadhyay, S. In-plane effective mass in narrow quantum wells of non-parabolic semiconductors. *Appl. Phys. Lett.* **1993**, *62*, 2416–2418.

(34) Wetzel, C.; Winkler, R.; Drechsler, M.; Meyer, B.; Rössler, U.; Scriba, J.; Kotthaus, J.; Härle, V.; Scholz, F. Electron effective mass and nonparabolicity in Ga 0.47 In 0.53 As/InP quantum wells. *Phys. Rev. B* **1996**, *53*, 1038.

(35) Haldar, S.; Dixit, V.; Vashisht, G.; Khamari, S. K.; Porwal, S.; Sharma, T.; Oak, S. Effect of carrier confinement on effective mass of excitons and estimation of ultralow disorder in Al x Ga 1- x As/GaAs quantum wells by magneto-photoluminescence. *Sci. Rep.* **2017**, *7*, 1–12.

(36) Çelik, H.; Cankurtaran, M.; Bayrakli, A.; Tiras, E.; Balkan, N. Well-width dependence of the in-plane effective mass and quantum lifetime of electrons in multiple quantum wells. *Semicond. Sci. Technol.* **1997**, *12*, 389.

(37) Städele, M.; Hess, K. Effective-mass enhancement and nonparabolicity in thin GaAs quantum wells. *J. Appl. Phys.* **2000**, *88*, 6945–6947.

(38) Zhang, L.; Liang, W. How the Structures and Properties of Two-Dimensional Layered Perovskites MAPbI 3 and CsPbI 3 Vary with the Number of Layers. *J. Phys. Chem. Lett.* **2017**, *8*, 1517–1523.

(39) Wang, Z.; Ganose, A. M.; Niu, C.; Scanlon, D. O. First-principles insights into tin-based two-dimensional hybrid halide perovskites for photovoltaics. *J. Mater. Chem.A* **2018**, *6*, 5652–5660.

(40) Paritmongkol, W.; Dahod, N. S.; Stollmann, A.; Mao, N.; Settens, C.; Zheng, S.-L.; Tisdale, W. A. Synthetic variation and structural trends in layered two-dimensional alkylammonium lead halide perovskites. *Chem. Mater.* **2019**, *31*, 5592–5607.

(41) Calabrese, J.; Jones, N. L.; Harlow, R. L.; Herron, N.; Thorn, D. L.; Wang, Y. Preparation and characterization of layered lead halide compounds. *J. Am. Chem. Soc.* **1991**, *113*, 2328–2330.

(42) Mitzi, D. B.; Dimitrakopoulos, C. D.; Kosbar, L. L. Structurally tailored organic-inorganic perovskites: Optical properties and solution-processed channel materials for thin-film transistors. *Chem. Mater.* **2001**, *13*, 3728–3740.

(43) Billing, D. G.; Lemmerer, A. Synthesis, characterization and phase transitions in the inorganic–organic layered perovskite-type hybrids [(CnH2n+ 1NH3) 2PbI4], n= 4, 5 and 6. *Acta Crystallogr., Sect. B: Struct. Sci* **2007**, *63*, 735–747.

(44) Whitfield, P. S.; Herron, N.; Guise, W. E.; Page, K.; Cheng, Y. Q.; Milas, I.; Crawford, M. K. Structures, phase transitions and tricritical behavior of the hybrid perovskite methyl ammonium lead iodide. *Sci. Rep.* **2016**, *6*, 35685.

(45) Miyata, A.; Mitioglu, A.; Plochocka, P.; Portugall, O.; Wang, J. T.-W.; Stranks, S. D.; Snaith, H. J.; Nicholas, R. J. Direct measurement of the exciton binding energy and effective masses for charge carriers in organic–inorganic tri-halide perovskites. *Nat. Phys.* **2015**, *11*, 582–587.

(46) Gauthron, K.; Lauret, J.-s.; Doyennette, L.; Lanty, G.; Al Choueiry, A.; Zhang, S. J.; Brehier, A.; Largeau, L.; Mauguin, O.; Bloch, J. et al. Optical spectroscopy of two-dimensional layered (C_6H_5C_2H_4-NH_3)_2-PbI_4 perovskite. *Opt. Express* **2010**, *18*, 5912.

(47) Delport, G.; Chehade, G.; Lédée, F.; Diab, H.; Milesi-Brault, C.; Trippe-Allard, G.; Even, J.; Lauret, J.-S.; Deleporte, E.; Garrot, D. Exciton–exciton annihilation in two-dimensional halide perovskites at room temperature. *J. Phys. Chem. Lett.* **2019**, *10*, 5153–5159.

(48) Galkowski, K.; Mitioglu, A.; Miyata, A.; Plochocka, P.; Portugall, O.; Eperon, G. E.; Wang, J. T.-W.; Stergiopoulos, T.; Stranks, S. D.; Snaith, H. J. et al. Determination of the exciton binding energy and effective masses for methylammonium and formamidinium lead tri-halide perovskite semiconductors. *Energy Environ. Sci.* **2016**, *9*, 962–970.

(49) Paritmongkol, W.; Powers, E. R.; Dahod, N. S.; Tisdale, W. A. Two origins of broadband emission in multilayered 2D lead iodide perovskites. *J. Phys. Chem. Lett.* **2020**, *11*, 8565–8572.

(50) Yang, Z.; Surrente, A.; Galkowski, K.; Bruyant, N.; Maude, D. K.; Haghighirad, A. A.; Snaith, H. J.; Plochocka, P.; Nicholas, R. J. Unraveling the exciton binding energy and the dielectric constant in single-crystal methylammonium lead triiodide perovskite. *J. Phys. Chem. Lett.* **2017**, *8*, 1851–1855.